Integrated silicon photodetector for lab-on-chip sensor platform

A. Samusenko[a,b], G. Pucker[b], D. Gandolfi[a], R. Guider[a], M. Ghulinyan[b], F. Ficorella[b], L. Pavesi[a].

[a]Department of Physics, University of Trento, Nanoscience Laboratory, Via Sommarive 14, Povo, Italy;

[b]Fondazione Bruno Kessler, Centre for Materials and Microsystems, Via Sommarive 18, Povo, Italy

ABSTRACT

In this paper we demonstrate design, fabrication and characterization of polycrystalline silicon (poly-Si) photodetectors monolithically integrated on top of a silicon oxynitride (SiON) passive photonic circuit. The devices are developed for operation at the wavelength of ∼850nm. Interdigitated PIN structures were designed and compared with conventional lateral PIN detectors. The devices, fabricated in standard CMOS technology, exhibit low dark current values of few nanoamperes. The best responsivity of 0.33A/W under a reverse bias of 9V was achieved for lateral PIN detectors with 3-μm interelectrode gap, coupled vertically to the optical waveguide. The applicability of devices for lab-on-chip biosensing has been proved by demonstrating the possibility to reproduce the sensor's spectral response.

Keywords: Silicon, optoelectronics, PIN photodetector, near-infrared, photonic integrated circuit

1. INTRODUCTION

In recent years, silicon photonics gains increasing interest as a platform for the realization of low-cost integrated optical devices by means of standard semiconductor fabrication techniques.[1] Hybrid and heterogeneous integration is the choice for fabrication of devices operating in the telecommunication windows at the wavelengths of approximately 1.3μm and 1.55μm. Also for lab-on-chip devices for biosensing a clear trend towards integrated optical devices is evident.[2] The on-chip integration of a photodetector, a critical component of any photonic device, is highly desirable to reduce packaging costs and to simplify integration. On-chip integrated detectors operating in the telecom windows have been mainly demonstrated using III-V and SiGe materials.[3–8] For lab-on-chip devices the near-infrared (NIR) spectral region between ∼750nm and 900nm represents an interesting alternative. In this case the passive optical circuits can be either realized in Si_3N_4 or SiO_xN_y, and the photodetector can be made out of silicon itself.

A variety of silicon based photodetectors operating at visible or short-wave near-infrared (SW-NIR) region have been investigated in the past.[9–11] In this paper we demonstrate waveguide-integrated lateral silicon PIN photodetectors developed for operation at the wavelength of ∼850nm. The devices are a part of an optical label-free biosensing chip based on whispering-gallery mode (WGM) resonators and integrated low-cost VCSEL diodes as light sources. The response time of this type of biosensor is usually in the range from some seconds to minutes caused by the slow analyte diffusion and bonding kinetics. Therefore we focus on the optimization of the photodetector's responsivity and not the speed. The design of the devices is fully compatible with standard CMOS microfabrication technology.

Further author information: (Send correspondence to S.A.)
S.A.: E-mail: samusenko@fbk.eu, Telephone: +39 0461 314 188

Integrated Photonics: Materials, Devices, and Applications III, edited by Jean-Marc Fédéli,
Proc. of SPIE Vol. 9520, 95200D · © 2015 SPIE · CCC code: 0277-786X/15/$18
doi: 10.1117/12.2178973

Downloaded From: http://proceedings.spiedigitallibrary.org/ on 06/03/2015 Terms of Use: http://spiedl.org/terms

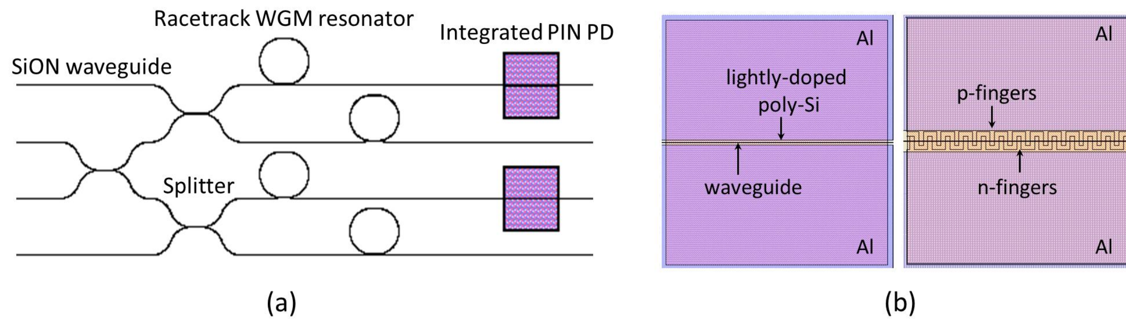

Figure 1. (a) CAD design of the WGM resonator-based photonic circuit with on-top integrated silicon PIN photodetectors. (b) Schematic of the integrated photodetectors: conventional lateral PIN detector (left) and interdigitated PIN detector (right).

2. EXPERIMENT

2.1 Device Design

Figure 1(a) shows the design of a SiON-based planar photonic circuit consisting of an array of identical WGM resonators laterally coupled to the straight waveguides. The resonators have a racetrack geometry with a bend radius of 100μm which guaranties negligible radiation losses. Directional couplers are used to split the light into four arms. This circuit represents a simple model of an optical biosensor based on the detection of refractive index change in the evanescent part of the field. The single mode SiON waveguide is designed in a way to provide an extension of the evanescent tail of the guided mode beyond the waveguide boundaries. The variation of the effective refractive index manifests as the shift of the resonance wavelength in the spectrum of the WGM resonator, which is then monitored with a photodetector.

The PIN detectors are integrated on top of two of the output waveguides. Figure 1(b) shows the design of two types of the photodetectors: conventional lateral PIN detectors with 3-μm and 5-μm gap between p^+/n^+ regions (left) and interdigitated PIN structures with finger spacing of 5μm (right). Interdigitated configuration allows extension of the device active area while keeping shorter distance between the p^+/n^+ "fingers", so that the carriers drifting across the depletion zone are able to reach the electrodes before the they recombine. Consequently, this benefits carriers collection and results in higher values of the photogenerated current.

To examine the waveguide-detector coupling mechanism we performed FEM/FDTD simulations with a simple film-like detector structure on top of the waveguide considering the following parameters: the SiON waveguide with refractive index of 1.66 has the dimensions of 1μm x 300nm, detector thickness is 150nm, the poly-Si refractive index is 3.6+i0.0014. The waveguide and the detector interact through the evanescent coupling of the waveguide fundamental mode with the modes excited in the detector layer. An additional SiO_2 layer of 50nm was introduced between the waveguide and the detector. Simulations showed that this layer helps to reduce the scattering towards the substrate in the interface between the films.

As light propagates through the waveguide, it is absorbed upward along the detector length which was chosen to be 150μm. This value is several times the minimum length obtained from simulations to couple over 95% of photons from the waveguide to the detector. In the end of the poly-Si slab, the light, still guided in the waveguide, can scatter back in the detector due to abrupt refractive index change and favour the absorption efficiency. On the contrary, in the initial region of the waveguide-detector interaction the high refractive index contrast (1.66 vs. 3.6) impedes the efficient light coupling. Indeed, the simulations evidenced a strong reflection in the region where light impinges on the edge of the detector. The reduction of the scattering can be achieved by controlled etching of a via into the upper cladding to transform the waveguide-detector interface from vertical to inclined, resulting in a less abrupt change of refractive index in the "coupling area" as shown in Fig. 2.

Downloaded From: http://proceedings.spiedigitallibrary.org/ on 06/03/2015 Terms of Use: http://spiedl.org/terms

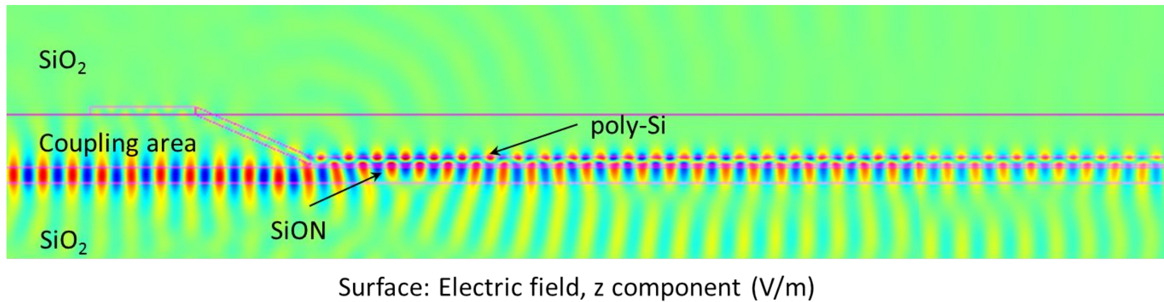

Figure 2. COMSOL simulation of light coupling from the waveguide into the thin photodetector layer. The reduction of scattering at the waveguide-detector interface is achieved by controlled etching of a via into the upper cladding.

2.2 Fabrication

The devices were fabricated on 6-inch silicon substrates with a 4μm thick layer of thermal silicon oxide. High quality SiON films were deposited by plasma-enhanced chemical vapour deposition (PECVD). The waveguides and the resonators were defined by standard UV-photolithography and reactive-ion etching followed by a high temperature annealing step to reduce the OH- and NH- groups in the SiON, and were then covered with TEOS silicon oxide deposited by LPCVD. To open the contact holes into the cladding and to provide the correct side-wall angle of the via, the samples were annealed and then etched in buffered HF solution. A thin film of TEOS (50nm) was deposited over in order to create the gap between the waveguide and the detector. Polysilicon films were deposited by low-pressure chemical vapour deposition (LPCVD) and lightly doped with boron (dose of 10^{12}atoms/cm^2). The patterned devices were then wet-etched in polysilicon etchant ($HNO_3/H_2O/HF$). The p^+ and n^+ regions were defined as contact holes in the photoresist, implanted by boron and phosphorous respectively (doses of $2\text{x}10^{15}$atoms/cm^2) and annealed at 900^0C for 30 minutes to activate the dopants. For realization of the contact metal pads, 500nm of pure aluminium was deposited by sputtering. After photolithography and etching, the wafers were annealed at 400^0C for 1 hour in H_2 atmosphere. Finally, the wafers were diced in chips along the lines, preliminary defined by silicon dry etching. SEM images of the fabricated devices are shown in Fig. 3.

2.3 Characterization

At first, electrical resistivity of device materials, polysilicon and aluminium, were investigated by means of measurement on standard microelectronic test structures, such as Van-der-Pauw cross and metal runner. The resistivity of doped polysilicon, dependent on the actual doping concentration, should be essentially low for PIN photodetector application. We obtained the bulk resistivities of $4\text{x}10^{-3}\Omega \cdot cm$ and of $7\text{x}10^{-3}\Omega \cdot cm$ for p-type and

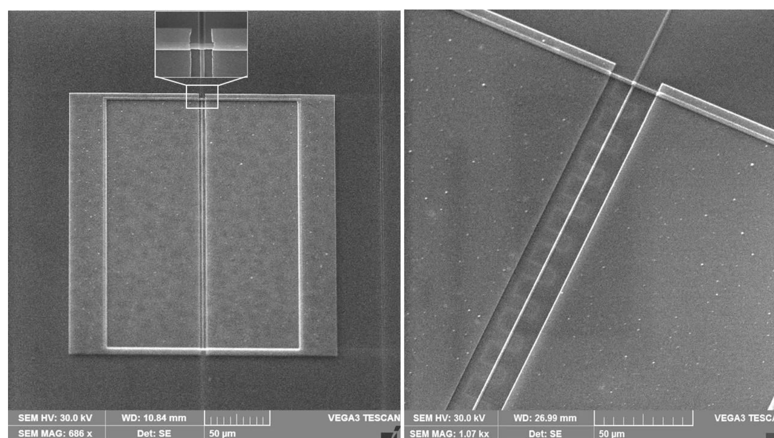

Figure 3. SEM images of the realized integrated PIN detectors: conventional (left) and interdigitated (right).

Downloaded From: http://proceedings.spiedigitallibrary.org/ on 06/03/2015 Terms of Use: http://spiedl.org/terms

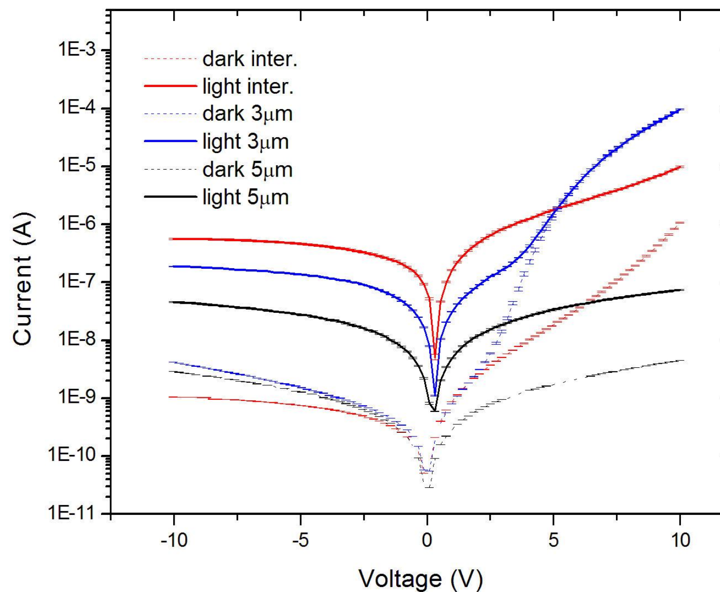

Figure 4. I-V characteristics of PIN photodetectors measured at top-illumination conditions.

n-type poly-Si respectively, while the resistivity of lightly-doped one was too low to be measured. These results are comparable with the data reported in literature for similar doping concentrations. Electrical resistivity of aluminium was found to be $2.7\text{x}10^{-8}\Omega \cdot m$, which is a typical value reported for pure aluminium deposited by sputtering.

The first insight into the electrical characteristics of the devices was provided by I-V characterization in the dark environment and under illumination from top with a 35mW laser emitting at 532nm. The diameter of the spot was ∼2mm, much larger than the active region of the detector. The I-V characteristics of PIN photodetectors are shown in Fig. 4. All the devices demonstrate a typical PIN photodiode behaviour and exhibit low values of dark current (less than 5nA). Interdigitated PIN detectors demonstrated the best values of photo-to-dark current ratio (∼500) for a broad range of reverse bias voltage under this particular illumination conditions. As it was mentioned above, this advantage is a result of the larger device depletion region and effective carrier collection by finger-like electrodes. Considering the area of illumination, the highest value of photocurrent density of 44mA/cm^2 was obtained for devices with 3-μm gap between electrodes.

Figure 5 (top) shows the experimental setup used to investigate the performance of detector in waveguiding configurtion. A function generator (FG) serves to form a sawtooth signal at the VCSEL diode input. TE polarized light from the VCSEL was launched into the input waveguide of the photonic chip through the fiber. The diode can be tuned in wavelength around 850nm by changing the driving current. An oscilloscope was used to measure the output voltage signal in time domain from both the integrated PIN detectors and the reference fiber-coupled commercial photodetector (PD). Considering the detector load resistance, the voltage was then translated into the current signal varying with the output wavelength of VCSEL. We present the results of the measurements on the PIN detector with 3-μm interelectrode gap which has demonstrated the highest value of photocurrent density under illumination from top and best repeatability of measurements in waveguiding configuration.

In Fig. 5 (bottom) we show the spectra obtained with the experimental setup explained before. The current-wavelength curves reported show an increase in current for longer wavelengths due to the change in bias applied to the VCSEL used to drive the diode in wavelength. Superimposed on the continuously increasing current, one observes the WGM resonances as dips in the spectra. The chip was designed in a way that, when the optical

Downloaded From: http://proceedings.spiedigitallibrary.org/ on 06/03/2015 Terms of Use: http://spiedl.org/terms

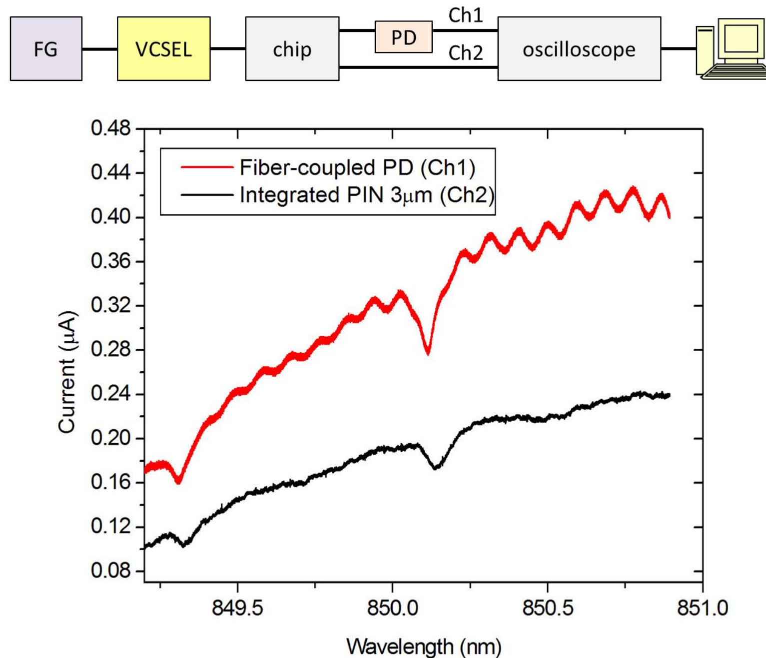

Figure 5. (top) Schematic diagram of the experimental setup for simultaneous measurement of current signal from an external fiber-coupled photodiode as well as from the integrated PIN detector. (bottom) Obtained output spectrum of the WGM resonator-based circuit.

signal is coupled to the resonator, a drop of the waveguide transmission signal occurs. The resonance quality factors were estimated to be around 13,000. For both cases of acquisition (internal and external detector) WGM resonances at wavelengths of 849.3nm and 850.1nm are clearly visible. The observed free spectral range (FSR) of 0.8nm is in reasonable agreement with the free spectral range of 0.7nm obtained in our design study of the optical circuit. This experiment proofs that our integrated PIN detectors may be used to monitor the optical signals in the sensor circuit.

The responsivity of the integrated photodetector ($\Re = I_{ph}/P_{in}$) was estimated as explained in the flowing. I_{ph} is the photocurrent measured with the detector subtracting the device dark current of 5nA. The input optical power (P_{in}) was approximated to the one measured with the reference photodetector (0.7μW), assuming the same optical power losses from the diode to the detectors, as for fiber-coupled photodiode so for the integrated photodetector. The average responsivity of 0.33A/W was obtained for the wavelengths around 850nm. The calculated external quantum efficiency is found to be 0.5.

3. CONCLUSION

We developed a series of CMOS compatible polysilicon photodetectors integrated on top of a silicon oxinitride photonic circuit. The best devices (conventional lateral PIN detectors with 3-μm interelectrode gap) have shown the responsivity of 0.33A/W at wavelength around 850nm which corresponds to the external quantum efficiency of 0.5. The ability to reproduce the spectrum of the WGM resonators was proved experimentally, demonstrating that the biosensor response can be monitored with presented integrated photodetectors. The performance characteristics of the device are comparable with commercial VIS-NIR silicon photodiodes.

ACKNOWLEDGMENTS

This work was supported by the FP7 EU project Symphony (Grant agreement no: 610580).

Downloaded From: http://proceedings.spiedigitallibrary.org/ on 06/03/2015 Terms of Use: http://spiedl.org/terms

REFERENCES

[1] Heck, M., Bauters, J., Davenport, M., Doylend, J., Jain, S., Kurczveil, G., Srinivasan, S., Tang, Y., and Bowers, J., "Hybrid silicon photonic integrated circuit technology," *Selected Topics in Quantum Electronics, IEEE Journal of* **19**(4), 6100117–6100117 (2013).

[2] Estevez, M., Alvarez, M., and Lechuga, L., "Integrated optical devices for lab-on-a-chip biosensing applications," *Laser Photonics Reviews* **6**(4), 463–487 (2012).

[3] Yuan, G., Pownall, R., Nikkel, P., Thangaraj, C., Chen, T., and Lear, K., "Characterization of cmos compatible waveguide-coupled leaky-mode photodetectors," *Photonics Technology Letters, IEEE* **18**(15), 1657–1659 (2006).

[4] Ahn, D., yin Hong, C., Liu, J., Giziewicz, W., Beals, M., Kimerling, L. C., Michel, J., Chen, J., and Kärtner, F. X., "High performance, waveguide integrated ge photodetectors," *Opt. Express* **15**(7), 3916–3921 (2007).

[5] Brouckaert, J., Roelkens, G., Thourhout, D. V., and Baets, R., "Thin-film iii–v photodetectors integrated on silicon-on-insulator photonic ics," *J. Lightwave Technol.* **25**(4), 1053–1060 (2007).

[6] Gan, X., Shiue, R.-J., Gao, Y., Meric, I., Heinz, T. F., Shepard, K., Hone, J., Assefa, S., and Englund, D., "Chip-integrated ultrafast graphene photodetector with high responsivity," *Nat Photon* **7**(11), 883–887 (2013).

[7] Ahn, D., Kimerling, L. C., and Michel, J., "Evanescent coupling device design for waveguide-integrated group iv photodetectors," *J. Lightwave Technol.* **28**(23), 3387–3394 (2010).

[8] Chen, L., Dong, P., and Lipson, M., "High performance germanium photodetectors integrated on submicron silicon waveguides by low temperature wafer bonding," *Opt. Express* **16**(15), 11513–11518 (2008).

[9] MacDonald, R., Tarr, N., Syrett, B., Boothroyd, S., and Chrostowski, J., "Msm photodetector fabricated on polycrystalline silicon," *Photonics Technology Letters, IEEE* **11**(1), 108–110 (1999).

[10] Ciftcioglu, B., Lin, Z., Jie, Z., Marciante, J. R., ZuegelL, J., Sobolewski, R., and Hui, W., "Integrated silicon pin photodiodes using deep n-well in a standard 0.18-μm cmos technology," *Journal of lightwave technology* **27**(13-16), 3303–3313 (2009).

[11] Dhar, S., Miller, D. M., and Jokerst, N. M., "High responsivity, low dark current, heterogeneously integrated thin film si photodetectors on rigid and flexible substrates," *Opt. Express* **22**(5), 5052–5059 (2014).

Downloaded From: http://proceedings.spiedigitallibrary.org/ on 06/03/2015 Terms of Use: http://spiedl.org/terms